

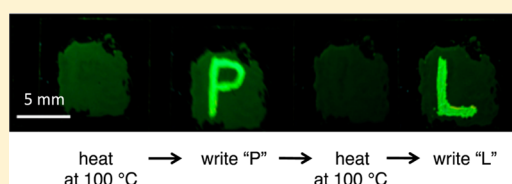
Crystal Structures, Thermal Properties, and Emission Behaviors of *N,N*-*R*-Phenyl-7-amino-2,4-trifluoromethylquinoline Derivatives: Supercooled Liquid-to-Crystal Transformation Induced by Mechanical Stimuli

Satoru Karasawa, Ryusuke Hagihara, Yuichiro Abe, Naomi Harada, Jun-ichi Todo, and Noboru Koga*

Graduate School of Pharmaceutical Sciences, Kyushu University, 3-1-1 Maidashi, Higashi-Ku, Fukuoka 812-8582, Japan

Supporting Information

ABSTRACT: *N,N*-*R*-Phenyl-7-amino-2,4-trifluoromethylquinoline derivatives (*R* = Me (1), Et (2), isopropyl (3), and Ph (4)) were prepared as a new type of fluorophore responsive to external stimuli. 1, 2, 3, and 4 were obtained as single crystals including three crystal polymorphs (1α , 1β , and 1γ) of 1 and two (2α and 2β) of 2. In 4, a phase transition from 4_{173} and 4_{90} between 173 and 90 K was observed. The solid-state emission showed a red shift by 30–58 nm compared with the emission in *n*-hexane, and their emission properties depended on the molecular arrangements. The modes of molecular arrangements for 1α , 1β , and 1γ were a slipped parallel (SP), head-to-tail γ -type herringbone (HT- γ -HB), and head-to-head γ -type herringbone (HH- γ -HB); those for 2α and 2β were HT- γ -HB and head-to-tail dimer (HT-dimer), and that for 3 was head-to-tail columnar (HTC). 4_{173} and 4_{90} were similar HT- γ -HB. The crystal-to-crystal transformations from 1γ to 1β and from 2β to 2α were observed by heating and grinding the crystal, respectively, with emittance changes. After melting, on cooling, all crystals formed supercooled liquid (SCL) and then glass states. In the SCL state, molecules were amorphous and were quickly crystallized by a mechanical stimulus such as scratching. By taking advantage of the difference of emitting intensity between the SCL and the crystal states for 1, “writing” and “erasing” of a letter with scratching and heating, respectively, were demonstrated.



INTRODUCTION

Organic molecules and metal complexes showing solid-state emission have attracted much interest as new functional materials for practical application in electronic and photo-devices,¹ photosensors,² and solid lasers.³ The characteristic of solid-state emission is that the emission behavior is strongly affected by the molecular structure and arrangement in the solid state. The wavelength and intensity of the solid-state emission can thus be reversibly tuned and controlled by altering the molecular structure and arrangement by external stimuli.⁴ In such solid-state emission alteration, strategies taking advantage of crystal-to-crystal (C-to-C) phase transitions in polymorphs are a promising approach, and many studies on the emission alteration induced by thermal⁵ and mechanical^{4a,6} stimuli have been reported. We have also reported on the solid-state emissions of 7-amino-2,4-ditrifluoromethylquinoline (TFMAQ) derivatives⁷ and analogous 1,8-naphthyridine derivatives.⁸ They provided many crystal polymorphs⁹ and exhibit polymorph-dependent emissions through the thermal single-crystal-to-single-crystal (SC-to-SC) phase transitions between the polymorphs. Along the studies on thermal interconversion between the polymorphs, furthermore, we found that a TFMAQ derivative formed a supercooled liquid (SCL) state after melting. Since the molecule in the SCL state subsequently crystallized, we considered using an SCL-to-C transformation by external stimuli as a new function of the emitting molecule. Although in the field of organic light-

emitting diodes (OLEDs) the SCL-to-C transformation is one of the problems for amorphous molecular materials,¹⁰ the difference in the emission color or intensity caused by SCL-to-C transformation by external stimuli was expected to be useful as a switching device for solid-state emitting materials. On the basis of the TFMAQ studies, fluorophore molecules incorporating diarylamine moieties being apt to form a SCL state¹¹ into a TFMAQ framework were prepared, and the alterations of emission properties through the phase transition from SCL to C caused by external stimuli were investigated. We report herein the preparations of TFMAQ derivatives having phenyl and *R*, Me (1), Et (2), isopropyl (3), and Ph (4), as substituents at the amino moiety, the molecule and crystal structures of their crystal polymorphs, and the mechanochromic emission alterations through the SCL-to-C phase transition. In addition, the thermal and mechanochromic emission alterations through C-to-C phase transition are reported.

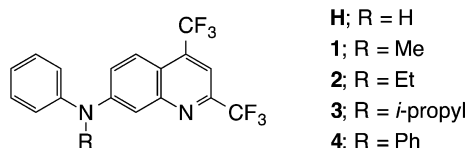
RESULTS AND DISCUSSION

Preparations of *N*-Phenyl TFMAQ Derivatives. To investigate the substituent effect on the SCL state, different sizes of substituents, methyl (1), ethyl (2), isopropyl (3), and

Received: February 4, 2014

Revised: March 20, 2014

Published: March 31, 2014



phenyl (**4**) moieties, were incorporated into 2,4-difluoro-7-phenylaminoquinoline (**H**). A parent molecule, **H**, prepared by the procedure reported previously⁷ was methylated with methyl iodide in the presence of sodium hydride to afford **1**. Similarly, **2** and **3** were prepared in a manner similar to the procedure for **1** using ethyl iodide and 2-iodopropane in place of methyl iodide. Fluorophore **4** was prepared by the reaction of **H** with bromobenzene in the presence of tri-*tert*-butylphosphine/palladium acetate/potassium *tert*-butoxide under a nitrogen atmosphere. Fluorophore **1** was crystallized to give three kinds of single crystals as yellowish plates (crystal **1 α**) and needles (crystal **1 β**) from *n*-hexane–Et₂O at 4 °C and rt, respectively, and yellowish needles (crystal **1 γ**) from acetone–Et₂O at rt. Crystals **1 β** and **1 γ** showed similar morphologies and emitting colors and could not be distinguished (Figure S1, Supporting Information). Recrystallization of **2** afforded crystal of **2 α** as yellowish needles from *n*-hexane–Et₂O and crystal of **2 β** as yellowish plates from ethyl acetate. Two crystals, **2 α** and **2 β** , emitted a yellowish green and a green color, respectively, and could be visually told apart by the emission colors. Single crystals of **3** and **4** were obtained from *n*-hexane–Et₂O as yellowish blocks. Photographs of crystals, **1–4**, irradiated by light at 365 nm under a microscope ($\times 40$) are shown in Figure S1.

Crystal Structure Analyses. The molecular and crystal structures for **1**, **2**, **3**, and **4** were investigated by single-crystal X-ray diffraction (SXRD) at various temperatures (273 and 90 K for **1**, **2**, and **3**, and 273, 223, 173, and 90 K for **4**). In X-ray crystallography at both temperatures, **1**, **2**, and **3**, showed no significant differences in cell parameters, while **4** showed a

drastic change of the crystal parameters with space group and crystal class between 173 and 90 K, suggesting thermal crystal phase transition. The molecules crystallized in space groups (crystal class), $P\bar{1}$ (triclinic), $C2/c$ (monoclinic), and Cc (monoclinic), for **1 α** , **1 β** , **1 γ** , respectively, $Pna2_1$ (orthorhombic) and $P\bar{1}$ (triclinic), for **2 α** and **2 β** , respectively, $P2_1/c$ for **3**, and $C2/c$ (monoclinic) and $P\bar{1}$ (triclinic) at 173 and 90 K for **4**₁₇₃ and **4**₉₀, respectively. In **1**, the Z' values for crystals **1 α** and **1 γ** were 2, indicating that the both crystals had two crystallographically independent molecules. In **2**, the Z' values for **2 α** and **2 β** were 2 and 1, respectively, and that value for **3** was 1. In **4**, the Z' value of 1 at 173 K increased to 4 by decreasing temperature to 90 K, suggesting that the symmetry of the crystal decreased with decreasing the temperature. Crystallographic data and experimental details are listed in Table S1 for **1**, S2 for **2** and **3**, and S3 for **4** in Supporting Information (S2).

The three crystals, **1 α** , **1 β** , and **1 γ** , for **1** showed similar molecular structures, in which the phenyl ring located in the side of the nitrogen atom of quinoline (syn conformer) and the disorders of phenyl rings were observed in **1 β** and **1 γ** . On the other hand, the crystal polymorphs, **2 α** and **2 β** , for **2** had a phenyl ring on the opposite side from each other (syn and anti conformers for **2 α** and **2 β** , respectively), and no disorders of the phenyl rings were observed in either molecule. **3** as well as **2 β** was an anti conformer. In **4**, two phenyl rings and one quinoline ring were tilted in the same direction to form a propeller shape.¹² The molecular structures are shown in Figure 1 for **1 α** , **2 β** , **3**, and **4**₉₀ and Figure S2, Supporting Information for **1 β** , **1 γ** , **2 α** , and **4**₁₇₃.

In **1**, **2**, **3**, and **4**, no noticeable differences in the lengths and angles of molecular structures from those of the parent molecule **H** and the analogues reported previously⁷ were observed. The bond lengths, r_{C7-N_a} of C7 and N_a of amine were 1.37–1.39 Å and were somewhat shorter, suggesting the double bond character. The dihedral angles of the quinoline

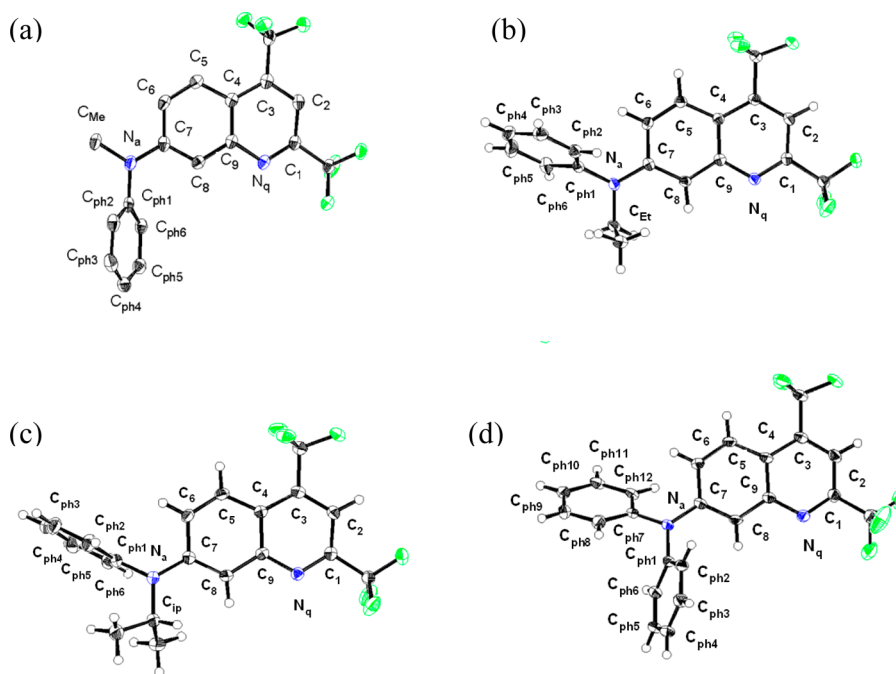


Figure 1. ORTEP drawings of the molecular structures of **1 α** (a), **2 β** (b), **3** (c), and **4**₉₀ (d) at 50% probability level. In (a) and (b), one of two and four crystallographically independent molecules of **1 α** and **4**₉₀ are shown.

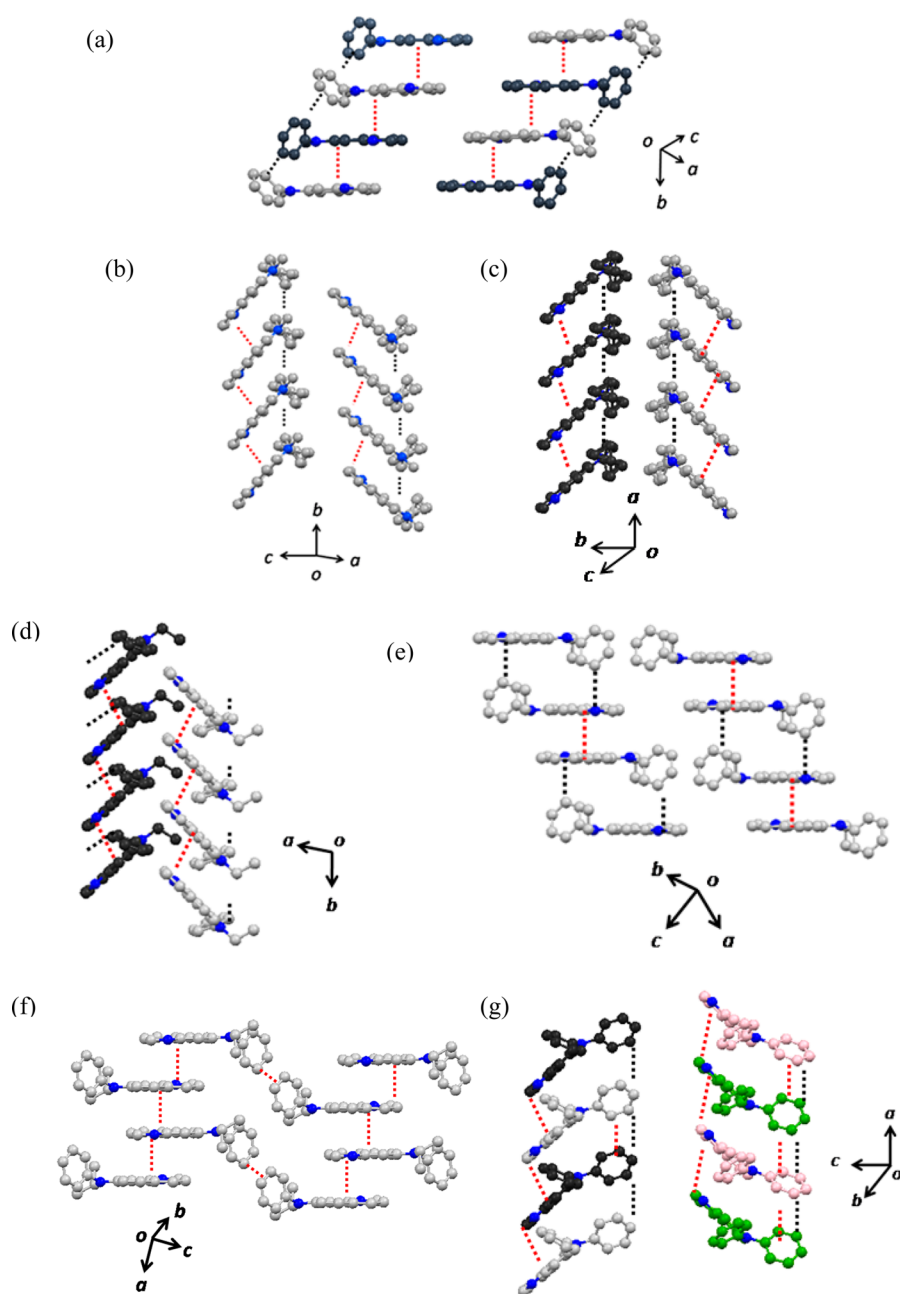


Figure 2. Molecular arrangements of crystals, **1 α** (a), **1 β** (b), **1 γ** (c), **2 α** (d), **2 β** (e), **3** (f), and **4 $_{90}$** (g). Gray, black, pink, and green molecules and blue atoms indicate crystallographically independent molecules and nitrogen atoms, respectively. Red and black dotted lines indicate short distances due to the π - π and CH- π interaction, respectively.

(Q) and phenyl rings toward the planes defined by the carbons of benzene and alkyl moieties and the nitrogen of amine increased in the order of **1**, **2**, **3**, and **4**, depending on the bulkiness of substituents (methyl, ethyl, isopropyl, and phenyl moieties). The dihedral angles, $C_{\text{Ph}1'}-N_a-C_R-Q$; C_R = the carbon of substituent R attached to the amine nitrogen, were 3.5 – 7.6° , 6 – 17° , and 24° for **1**, **2**, and **3**, respectively, which corresponded to the torsion angles, $\angle C_6-C_7-N_a-C_{\text{Ph}1'}$ and $C_7-N_a-C_R-\text{Ph}$ were 55 – 64° , 62 (64) $^\circ$, and 70° for **1**, **2**, and **3**, respectively. The small former angles suggested that the charge transfer effectively took place in the excited state. The latter large dihedral angles might affect the crystal packings. In **4**, two phenyl rings and one quinoline plane were tilted by 28 , 58 , and 73° , respectively, toward the plane defined by C7, Ph1,

and Ph1'. The selected bond lengths, bond angles, and dihedral angles for **1**, **2**, **3**, and **4 $_{90}$** are summarized in Tables S4-1 and S4-2, Supporting Information.

The molecular arrangements for **1**, **2**, **3**, and **4** were different layered structures. In **1**, the modes of molecular arrangement¹³ for **1 α** , **1 β** , and **1 γ** were a slipped parallel (SP), head-to-tail γ -type herringbone (HT- γ -HB), and head-to-head γ -type herringbone (HH- γ -HB), respectively. Those for **2 α** and **2 β** were HT- γ -HB and head-to-tail dimer (HT-dimer), respectively, and that for **3** was a head-to-tail columnar (HTC). **4 $_{173}$** and **4 $_{90}$** were similar HT- γ -HB. The molecular arrangements for **1 α** , **1 β** , **1 γ** , **2 α** , **2 β** , **3**, and **4 $_{90}$** are shown in Figure 2 (Figure S3, Supporting Information for **4 $_{173}$**).

Table 1. Modes of Molecular Arrangements and Intermolecular Distances and Angles for **1 α** , **1 β** , **1 γ** , **2 α** , **2 β** , **3**, and **4 a**

1α	1β	1γ	2α	2β	3	4$_{173}$	4$_{90}$
Space Group (Z')							
P $\bar{1}$ (2)	C $_2/c$ (1)	Cc (2)	Pna2 $_1$ (2)	P $\bar{1}$ (1)	P2 $_1/c$ (1)	C $_2/c$ (1)	P $\bar{1}$ (4)
Mode of Molecular Arrangement							
SP	HT- γ -HB	HH- γ -HB	HT- γ -HB	HT-dimer	HT-C	HT- γ -HB	HT- γ -HB
Intercentroid Distances between the Quinoline Ring							
4.73, 5.16	4.95	4.93	4.79	3.60	3.59	5.08	4.90–5.16
Nearest Distance (\AA) between the Quinoline and Benzene Planes for π - π Interactions							
C9–C6' 3.61	Na–C7' 3.53	Na–C7' 3.62	Na–C8' 3.47	C1–C6' 3.53	C5–C1' 3.62	Na–C6'' 3.76	Na–C6'' 3.62
C7–C3'' 3.65	C2–C5'' 3.53	Na''–C7''' 3.62	C8–Na' 3.48		C8–C5'' 3.66		C $_{ph3}''''$ –C $_{ph6}''''$ 3.42
Nearest Distance between the H of Phenyl Ring and Aromatic Planes for CH- π Interactions							
C $_{ph1}$ –H $_{ph2}'$ 3.08	C $_{ph1}$ –H $_{ph2}'$ 3.01	C $_{ph3}$ –H $_{ph3}'$ 2.64	C $_{ph5}$ –H $_{ph5}''$ 2.80	Na–H $_{ph5}''$ 2.71		C $_{ph11}$ –H $_{ph9}''$ 2.67	C $_{ph9}$ –H $_{ph9}^b$ 2.66–2.74
C $_{ph1}$ –H $_{ph2}''$ 3.30	C $_{ph4}$ –H $_{ph3}'$ 3.23	C $_{ph2}'$ –H $_{ph2}$ 2.75				C $_{ph8}$ –H $_{ph6}'$ 2.90	
CH–N Hydrogen Bonds							
H $_{ph4}$ –Nq 2.90, 3.01	H $_{ph4}$ –Nq 2.85	H $_{ph4}$ –Nq 2.60, 2.64	H $_{ph4}$ –Nq 2.91, 2.92	H $_{Et}$ –Nq 2.86	H $_{ph3}$ –Nq 2.82	H $_{ph4}$ –Nq 2.70	H $_{ph4}$ –Nq 2.62, 2.65, 2.68, 2.71

^aSP; a slipped parallel, HT; head-to-tail, HH; head-to-head, HB; herringbone, C; columnar. ^bIncludes six short distances of C $_{ph9}$ –H $_{ph9}''$, C $_{ph9}'$ –H $_{ph9}''$, C $_{ph9}''$ –H $_{ph9}'''$, C $_{ph9}'''$ –H $_{ph9}''''$, and C $_{ph9}''''$ –H $_{ph9}'''''$, respectively.

In layered structures such as columnar and herringbone, the CH- π interaction¹⁴ in addition to the π - π interaction effectively operates to stabilize the crystal structure. As shown in Figure 2, syn and anti conformers formed the head-to-head and head-to-tail layered structures of quinoline rings, respectively. A head-to-head structure for syn conformer could gain stability due to the CH- π interaction between the phenyl rings in addition to the π - π interaction between the quinoline rings. The formation of syn and anti conformers depended on the substituents, R, and the anti conformer became dominant with increasing bulkiness of R in the order of methyl, ethyl, and isopropyl. Three crystals, **1 α** , **1 β** , and **1 γ** , of **1** took syn conformation to form the SP and HB structures consisting of head-to-head overlaps of molecules. In **2**, **2 α** , and **2 β** took syn and anti conformation to form the HB- and HT-dimer structures consisting of head-to-head and head-to-tail overlaps, respectively. In the HT-dimer structure, interdimer short contacts for the CH- π interactions between the phenyl and quinoline rings were observed. Crystal **3** was obtained only as anti conformer and had a HT-C structure consisting of head-to-tail overlap. In this HT-C structure, the intercolumn short contacts between the phenyl rings, indicating the π - π interaction, were observed. **4** had a head-to-head overlap of quinoline rings to form the HB structure. In **4**, additional intermolecular π - π interactions between the phenyl rings were observed.

In **1**, **2**, **3**, and **4**, the intercentroid distances between quinoline rings estimated from the Mercury CSD 3.0 software¹⁵ were ca. 3.6–5.2 \AA , suggesting that the π - π interactions were weak. Furthermore, the short distances between the phenyl rings and between the phenyl and the quinoline rings indicating the CH- π interaction were 2.7–3.3 \AA , which might have stabilized the layered structures. The observed short contacts are shown in Figure 2, and their intermolecular distances and angles are summarized in Table 1 together with the molecular arrangement modes.

To confirm if three, two, and two kinds of crystals for **1**, **2**, and **4**, respectively, were polymorphous, the Hirshfeld fingerprint ($di - de$) plots¹⁶ were carried out. Those plots for **1**, **2**, and **4** are shown in Figure S4, Supporting Information. In visual comparisons of the Hirshfeld fingerprint plots, the molecules,

1 α -1 and **1 α -2**, and **1 γ -1** and **1 γ -2**, with $Z' = 2$, and **1 β** might look different from each other. Therefore, it was judged that **1** had three crystal polymorphs containing five crystallographically independent molecules. In contrast, the plots for **2 α** ($Z' = 2$) and **2 β** containing three crystallographically independent molecules were visually different, indicating that they were crystal polymorphs. The plots for **4 $_{173}$** and **4 $_{90}$** ($Z' = 4$) containing five crystallographically independent molecules were also visually different, indicating that they were crystal polymorphs.

Absorption and Emission Spectra. The absorption and emission properties of fluorophores **1**, **2**, **3**, and **4** were investigated in various solvents and in the solid state. The solid-state absorption spectra were obtained by measurements of the diffractive reflection spectra followed by Kubelka–Munk conversion. For the fluorescence spectra, the absorption maxima (370–400 nm) in the visible region were used as the excitation wavelength.

(A). *In Solutions.* The absorption and emission spectra of **1**, **2**, **3**, and **4** were measured in *n*-hexane, dibutyl ether, chloroform, ethyl acetate, and dimethyl sulfoxide (Figure S5, Supporting Information). Absorption spectra in the solution samples were similar to those for the TFMAQ derivatives reported previously.⁷ In *n*-hexane, the wavelengths of the charge transfer band were at $\lambda_{\max}^{\text{ab}} = 392, 398, 404, 402,$ and 415 nm for **H**, **1**, **2**, **3**, and **4**, respectively, and depended on the substituents. Solvent dependence of the $\lambda_{\max}^{\text{ab}}$ values was also observed, indicating that the molecules in the ground state were significantly polarized. The solutions of **1**, **2**, **3**, and **4** in organic solvents intensely emitted fluorescence, and the wavelength of the emission maximum, $\lambda_{\max}^{\text{f}}$, was longer compared with the parent molecule (**H**). In *n*-hexane, the emission for **H** was $\lambda_{\max}^{\text{f}}$ of 446 nm, while those for **1**, **2**, **3**, and **4** were $\lambda_{\max}^{\text{f}}$ of 471, 477, 472, and 479 nm with fluorescence quantum yields, Φ_{f} , of 0.49, 0.47, 0.31, and 0.63, respectively. The emission color and intensity depended on the solvent polarity. With increasing polarity, the $\lambda_{\max}^{\text{f}}$ for **1**, **2**, **3**, and **4** shifted to a longer wavelength, while the Φ_{f} values decreased. The observed emission properties in solution (solvatochromism)¹⁷ were typical of the fluorescence for TFMAQ derivatives. From the Lipper–Mataga model,¹⁸ the differences ($\Delta\mu$) between the

ground and excited state dipole moments for **1**, **2**, **3**, and **4** were estimated to be 14.9 (5.4), 14.7 (5.4), 14.7 (5.3), and 15.0 D (5.7), respectively, in which the numbers in the parentheses were Onsager Cavities estimated by density functional theory calculation using the B3LYP/6-31G(d) base set.¹⁹ The obtained values of 15 D were larger than that (12 D) for **H**, indicating that the photoexcited states for **1**, **2**, **3**, and **4** were largely stabilized by the polar solvent. The values of $\Delta\mu$, and λ_{\max}^f and Φ_f for **1**, **2**, **3**, and **4** in various solvents are listed in Table S5, Supporting Information together with those for the parent molecule **H**.

(B). *In the Solid State.* In the absorption spectra for the crushed crystalline samples, the $\lambda_{\max}^{\text{ab}}$ values of the long wavelength absorption were nearly constant by ca. 418 nm for **1 α** , **1 β** , **1 γ** , **2 α** , **2 β** , and **3** and 425 nm for **4** and showed red shifts, $\Delta\lambda_{\max}^{\text{ab}}$; $\lambda_{\max}^{\text{ab}}(c) - \lambda_{\max}^{\text{ab}}(n\text{-C}_6\text{H}_{14})$, of 10–20 nm compared with the corresponding values in *n*-hexane, where the contribution of stabilization by the solvent was negligible. In contrast, the λ_{\max}^f and Φ_f values of solid-state emission strongly depended on the molecular arrangements of crystals.²⁰ The λ_{\max}^f (Φ_f) values of the crystalline samples were 509 (0.52), 517 (0.51), and 520 (0.46) nm for **1 α** , **1 β** , and **1 γ** were 531 (0.40) and 510 (0.11) for **2 α** and **2 β** , and were 502 (0.10) and 537 (0.52) nm for **3** and **4**, respectively. When the solid-state emission properties were compared with those in *n*-hexane, the crystals, **1 β** , **1 γ** , **2 α** , and **4**, having HB structures showed large shifts to longer wavelengths by 46–58 nm, while crystals **2 β** and **3**, having HT-dimer and HT-C structures, respectively, showed smaller shifts by 33 and 30 nm with large reductions of Φ_f values. Crystal **1 α** having a slipped parallel arrangement showed an intermediate property. These observations were consistent with the results for the analogous 1-quinoline and 1,8-naphthyridine derivatives reported previously.^{7,8} Absorption and emission spectra of crushed crystalline samples are shown in Figure 3 for **1** and Figure S6, Supporting Information for **2**, **3**, and **4**. The values of $\lambda_{\max}^{\text{ab}}$, λ_{\max}^f , $\Delta\lambda_{\max}^{\text{f-ab}}$, and Φ_f are summarized in Table 2 together with those in *n*-hexane.

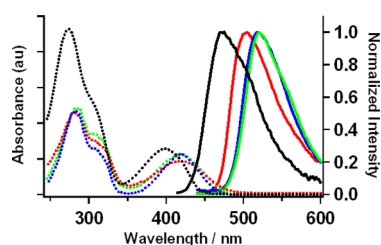


Figure 3. Solid-state absorption (dotted line) and emission (solid line) spectra for **1 α** (red), **1 β** (blue), and **1 γ** (green). Black lines show the spectra in *n*-hexane.

Thermal Properties. To investigate the thermal properties of **1**, **2**, **3**, and **4**, differential scan calorimetry (DSC) measurements were performed at heating and cooling rates of 10 and 5 °C/min in two temperature ranges: high ranges of 25–150, 0–100, 0–130, and 30–160 °C, and low ranges of –30 to 150, –40 to 100, –40 to 130, and –40 to 160 °C for **1**, **2**, **3**, and **4**, respectively. The observed DSC curves were different between the first and second scans. Furthermore, the second scan depended on the measuring temperature range. The DSC curves are shown in Figure 4 for **1 α** , **2 α** , **3**, and **4** and in Figure S7 for **1 β** , **1 γ** , and **2 β** .

In the high temperature range, crystals **1 α** and **1 β** showed a single endothermic peak at 98 °C, T_m , due to the melting point on heating in the first cycle, and no other peaks were observed in the second cycles, while crystal **1 γ** showed a weak endothermic peak at 89 °C, T_t (Figure S7b, Supporting Information) in addition to the peak of T_m in the first cycle, and no peaks were observed in the second cycles. The weak endothermic peak, T_p , might be due to the thermal phase transition, suggesting enantiotropic transformation^{8,21} to a polymorph from **1 γ** . Similar thermal profiles of DSC curves for **2**, **3**, and **4** were observed in the high temperature ranges. In the DSC curves of **2**, **3**, and **4**, only the endothermic peaks of T_m at 72 and 62 °C for **2 α** and **2 β** , respectively, and 94 and 118 °C for **3** and **4**, respectively, were observed in the first cycle, and no peaks were observed in the second cycle. Lack of any peak after melting in the first cycle for **1**, **2**, **3**, and **4** indicated that the samples were in a SCL state after melting. In the T_m values of polymorphs **2 α** and **2 β** , relatively large differences were observed, indicating that the molecules of syn conformer in HB structure for **2 α** were packed more tightly than those of anti conformer in HT-dimer for **2 β** .

In the low temperature ranges, on the other hand, the DSC curves of **1**, **2**, **3**, and **4** showed the peaks for T_g and T_s , due to the glass (G) transition and the solidification, respectively, in addition to that for T_m in the cooling and heating processes after melting. The DSC curves for **1** showed a weak and broad exothermic peak at –10 to 10 °C, T_g^- , in the cooling process following melting at 98 °C, and then a corresponding broad endothermic peak at –15 to –10 °C, T_g^+ , and an exothermic peak at 31 °C in the heating process from –30 °C. The observed pair of weak exo- and endothermic peaks and the exothermic peak at 31 °C, T_s , were assigned as the glass (G) transition and the solidification, respectively. The temperature of T_s depended on the heating rate, and the T_s value of 31 °C for 5 °C/min shifted to 40 °C for 10 °C/min. Furthermore, the exothermic peak at 40 °C was accompanied by an endothermic peak at 89 °C for T_t due to the phase transition (Figure S7a,b, Supporting Information), suggesting that the solid formed at T_s contained crystal **1 γ** . In **2 α** , after melting, a pair of weak exo- (endothermic) peaks for T_g^- (T_g^+) at –25 (–20) °C and a

Table 2. Values of Absorption and Emission Maxima ($\lambda_{\max}^{\text{ab}}$ and λ_{\max}^f , respectively), $\Delta\lambda_{\max}^{\text{f-ab}}$, and Φ_f for **1 α** , **1 β** , **1 γ** , **2 α** , **2 β** , **3**, and **4** in Crystalline State^a

	1α	1β	1γ	2α	2β	3	4
$\lambda_{\max}^{\text{ab}}/\text{nm}^b$	417 (398)	419 (398)	418 (398)	418 (404)	418 (404)	419 (402)	425 (415)
$\lambda_{\max}^f/\text{nm}$	509 (471)	517 (471)	520 (471)	531 (477)	510 (477)	502 (472)	537 (479)
$\Delta\lambda_{\max}^{\text{f-ab}}/\text{nm}$	92	98	102	92	113	83	112
Φ_f	0.52 (0.49)	0.50 (0.49)	0.46 (0.49)	0.40 (0.47)	0.11 (0.47)	0.10 (0.31)	0.52 (0.63)

^aThe numbers in the parentheses are those in *n*-hexane. ^bThe value obtained by measurements of the diffractive reflection spectra followed by Kubelka–Munk conversion.

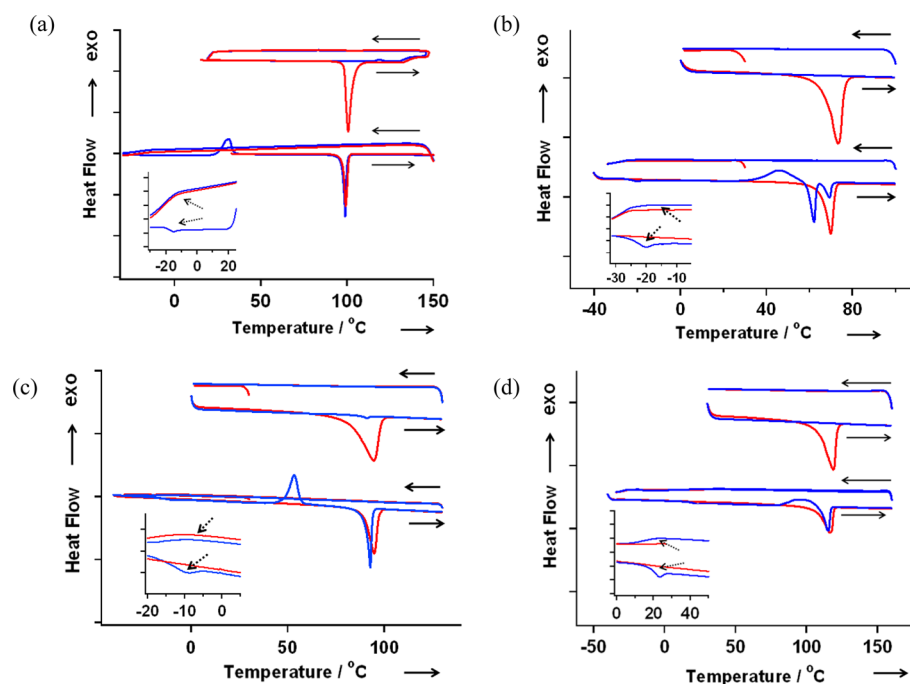


Figure 4. DSC curves of **1α** (a), **2α** (b), **3** (c), and **4** (d) for two cycles; first (red) and second (blue), in the high (upper) and low (bottom) temperature ranges; the high ranges of 25–150, 0–100, 0–130, and 30–160 °C, and the low ranges of –30 to 150, –40 to 100, –40 to 130, and –40 to 160 °C for (a), (b), (c), and (d), respectively. The rates of heating and cooling are 5 °C/min in (a) and 10 and 5 °C/min in the high and low temperature ranges, respectively, in (b), (c), and (d). Insets show the expansion in the temperature range observed at the glass transition. Solid and dotted arrows indicate the direction of heating and cooling, and the glass transition, respectively.

broad exothermic peak at 46 °C for T_s appeared, followed by the two endothermic peaks at 62 and 70 °C, which were consistent with the values of T_m for **2β** and **2α**, respectively. This result suggested that the solid formed at 46 °C was a mixture of **2α** and **2β**. The observed intensity ratio of the peaks of T_m for **2α** and **2β** depended on the scan rate, and the ratio of **2α/2β** decreased with decreasing scan rate. The intensity for **2β** became dominant at the scan rate of 1 °C/min (Figure S7d). This result suggested that **2α** and **2β** having modes of HB- and HT-dimer molecular arrangements might be kinetically and thermodynamically stable, respectively. Similarly, **3** and **4** showed pairs of weak exo- (endothermic) peaks for T_g^- (T_g^+) at –15 to 0 (–9) and 10–30 (23) °C, respectively, and followed by the broad exothermic peaks for T_s at 53 and 95 °C, respectively, just before reaching the melting point in the second cycle. The melting points in the second cycle for **3** and **4** were consistent with those for the first scan, indicating that the original **3** and **4** were solidified. It is noted that the T_g^+ value of **4** was 25 °C and relatively high, and **4** was in the G state near room temperature.

As shown in DSC measurements in the low temperature range, the sample via the G state spontaneously solidified from the SCL. The nucleus of a crystal might form in the G state and induce the crystallization in the SCL state. The values of T_m , T_g^- , and T_g^+ for **1**, **2**, **3**, and **4** are summarized in Table 3.

Emission Alteration with a Mechanical Stimulus. (A). *SCL-to-C Transformation.* As suggested by DSC, after melting, **1**, **2**, **3**, and **4** formed the SCL and G states at room temperature and below T_g . The samples in the G states were stable, while those in the SCL state were somehow labile depending on the fluorophore. The samples in SCL state were highly viscous oils, and the viscosity at room temperature increased in the order of $2 < 1 < 3 < 4$, which might correspond

Table 3. Values of T_m , T_v , T_s , T_g^- , and T_g^+ (°C), for **1**, **2**, **3**, and **4**^a

(°C)	1α	1β	1γ	2α	2β	3	4
T_m	98	98	n.d.	70	62	94	118
T_i			89				
T_s	31			46	53		~95
T_g^-	–10 to 10 (br)			n.d.		–15 to 0 (br)	10–30 (br)
T_g^+	–13			–20	–9		23

^a T_g^- and T_g^+ are in the cooling and heating process, respectively. n.d.; not determined.

to the order of T_g^+ . The obtained SCL state for **1** was maintained by leaving it at room temperature in a closed vessel for 1 week, and it had solidified 3 weeks later. **2** in the SCL state was relatively easily solidified after 24 h (Figure S8, Supporting Information). Photographs indicating the time dependence of transformation from SCL to solid at 20 ± 2 °C for **1–4** are shown in S8'. In contrast, upon scratching the surface of the viscous oil, the scratched part solidified and a bright emission was observed. Observation under a microscope suggested that solidification (crystallization) rapidly took place and then gradually and entirely expanded with time. The time dependence of solidification of **1** after scratching is shown in photographs in Figure 5.

The crystals were heated above T_m and the alterations of emission before and after scratching were examined using fluorescence spectroscopy. All samples in the SCL state showed emissions with similar wavelengths and Φ_f (540 ± 7 nm and 0.2, respectively). The emission showed red shifts of wavelengths by 21–32, 13–34, 34, and 10 nm for **1**, **2**, **3**, and **4**, respectively, and reduction of intensity except for **2β** and **3**, compared with the solid state. The observed red shifts of λ_{\max}^f and the reductions of Φ_f in the SCL state might suggest that the

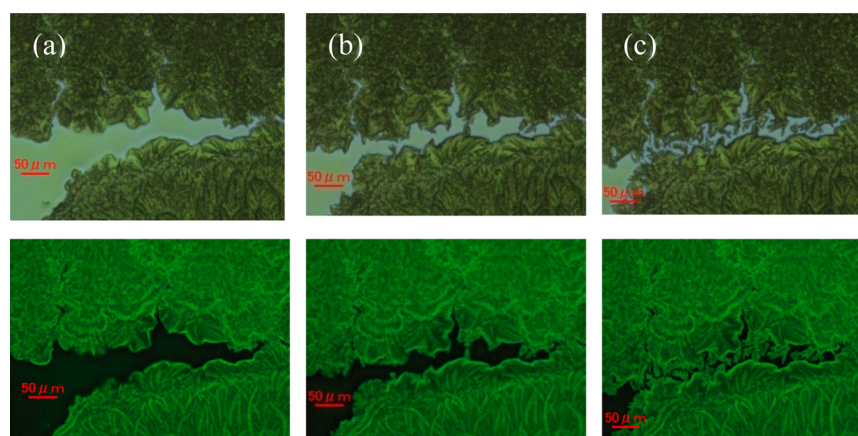


Figure 5. Photographs of **1** after scratching 15 (a), 20 (b), and 30 min (c) later. Upper and lower panels are under room light and light at 365 nm, respectively. In lower panels, the green and black area are solid and SCL parts, respectively.

intermolecular π - π interaction was stronger than that in the solid state. In contrast, the increase of Φ_f for **2 β** and **3** might be due to the molecular arrangements, columnar structures, becoming amorphous in the SCL state. The absorption and emission spectra of **1**, **2**, **3**, and **4** in the SCL state are shown in Figure S9, Supporting Information and the values of $\lambda_{\max}^{\text{ab}}$, $\lambda_{\max}^{\text{f}}$, and Φ_f are listed in Table 4.

Table 4. Values of Absorption and Emission Maxima ($\lambda_{\max}^{\text{ab}}$ and $\lambda_{\max}^{\text{f}}$, respectively) and Φ_f for **1**, **2**, **3**, and **4** in the SCL State

	1	2	3	4
$\lambda_{\max}^{\text{ab}}/\text{nm}$	412	417	416	430
$\lambda_{\max}^{\text{f}}/\text{nm}$	541	544	536	547
Φ_f	0.22	0.18	0.20	0.22

The sample of **1** in the SCL state showed a broad and weak emission at $\lambda_{\max}^{\text{f}}$ of 541 nm with $\Phi_f = 0.2$, while the scratched sample emitted an intense yellowish green ($\lambda_{\max}^{\text{f}} = 515$ nm). The fluorescence intensity increased more by annealing at 80 °C (10 min) for the complete solidification, and the obtained spectrum was similar to those for **1 β** and **1 γ** rather than **1 α** . Similarly, crystals, **2**, **3**, and **4** in the SCL state also showed alteration of their emission intensity in response to the mechanical stimuli. The observed emission intensity change could be repeated using the cycle of heating above T_m – scratching at room temperature, which are shown in Figure S10, Supporting Information. The rates of solidification in the SCL state after scratching were different and became faster in the order of **2** > **1** > **3** > **4**, which might correspond to the order of T_g^+ .

By taking advantage of the differences in the emission intensity depending on the state, that is, SCL or solid, writing and erasing were possible, as follows. The SCL of **1** emitted weakly. When the letter P was written by scratching several times with a fine wire, the letter P rapidly appeared under black light due to the crystallization at the stimulation point. With time, the letter P became blurred. Subsequently, when the temperature was raised to 100 °C and cooled to room temperature, the letter P disappeared and the sample returned to the SCL state. A different letter, L, was then written with a fine wire. The emission behavior of **1** in the cycle of heating and cooling is shown in Figure 6.

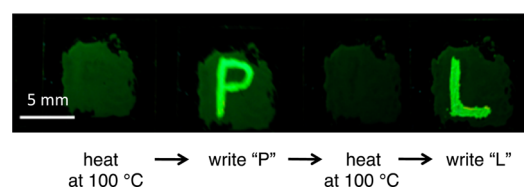


Figure 6. Photographs for **1** in the cycle of heating at 100 °C, cooling at 25 °C, and scratching. The letters “P” and “L” were written by scratching with a fine wire. The white scale bar indicates 5 mm.

2, **3**, and **4** also showed “write” and “erase” behaviors similar to **1** (Figure S11, Supporting Information). However, the written letters for **3** and **4** were not clear. In **3**, the difference of brightness between the letter and background was small because the Φ_f value in the crystal state was smaller than that in the SCL states. In **4**, on the other hand, the emission wavelengths in the crystal and SCL states were close to each other.

(B). C-to-C Transformation. Interestingly, the emitted green color for **2 β** in the crystalline state could be changed to yellowish green by grinding the crystal. In the emission spectra, the $\lambda_{\max}^{\text{f}}$ value of 510 nm shifted to ca. 530 nm after grinding, which was close to that for **2 α** , suggesting the formation of **2 α** through C-to-C transformation induced by mechanical stimuli. The spectral alterations before and after grinding **2 β** are shown in Figure S12, Supporting Information together with photographs under light at 365 nm. Furthermore, **2 β** also turned to **2 α** by exposure to CH_2Cl_2 vapor.²²

PXRD Measurements. To investigate the crystal structures of the products formed through SCL-to-C and C-to-C transformations, powder X-ray diffraction (PXRD) measurements were carried out. The obtained PXRD patterns for **1**, **2**, **3**, and **4** were consistent with those simulated by the data obtained from SXRD.

(A). SCL-to-C. PXRD patterns for **1 α** , **2 α** , **3**, and **4** were measured in various conditions. The alterations of PXRD patterns are shown in Figure 7 for **1 α** and **2 α** and Figure S13, Supporting Information for **3** and **4**.

After heating over mp and then cooling to 23 °C (30 °C for **4**) for **1 α** , **2 α** , **3**, and **4**, all sharp signals disappeared and broad signals were observed (Figure 7(a-ii) and (b-ii)), indicating that the samples were in the SCL state, which were amorphous. After scratching, the sharp signals appeared, indicating that the sample in SCL was crystallized. In **1 α** , the observed PXRD

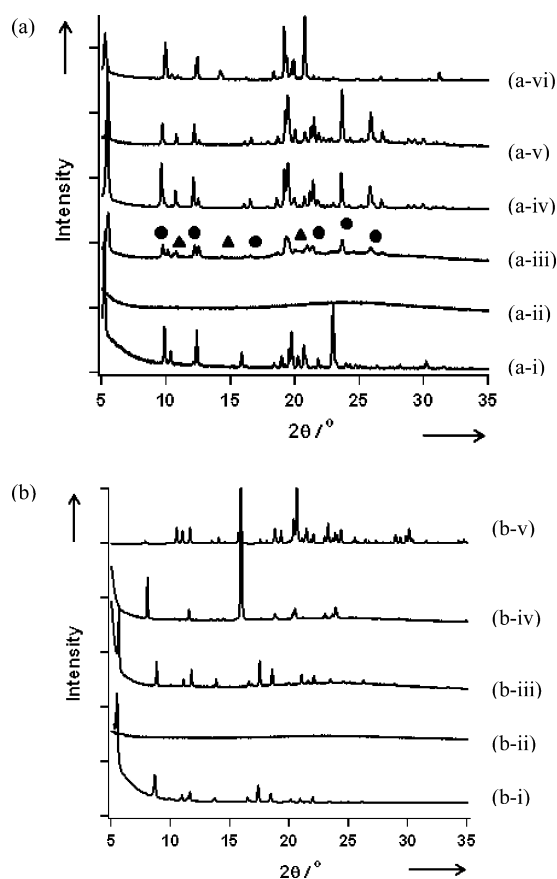


Figure 7. PXRD patterns of **1α** (a) and **2α** (b) under various conditions. For (a), before (a-i) and after heating at 100 °C (a-ii), after scratching (a-iii), after annealing at 80 °C for 10 min (a-iv), and those for crystal **1β** (a-v) and **1γ** (a-vi). Circles and triangles in (a-iii) indicate the peaks due to crystals **1β** and **1γ**, respectively. For (b), before (b-i) and after heating at 100 °C (b-ii), after scratching (b-iii), after leaving SCL for 6 h. (b-iv), and simulation of **2β** (b-v).

signal pattern after scratching suggested that a mixture of crystal **1β** and **1γ** formed (Figure 7(a-iii)). After annealing at 80 °C (Figure 7(a-iv)), the signals due to crystal **1γ** disappeared, and the signals due to crystal **1β** remained. In a separate PXRD experiment, a thermal transformation from **1γ** to **1β** was confirmed (Figure 8a). In **2α**, the PXRD patterns after scratching were consistent with those before heating the samples, indicating that **2α** was recovered. In contrast, when the sample in the SCL state was left for 6 h without scratching, a new pattern, which was consistent with that for **2β**, appeared (Figure 7(b-iv)). In the initial stage of scratching **3** in the SCL state, a new PXRD pattern in addition to the one for **3** appeared, while in the final stage the new pattern disappeared, and the original one for **3** remained. The observed new pattern might be due to a polymorph of **3**. At the present stage, a polymorph of **3** has not been isolated. The PXRD patterns for **3** and **4** were obtained after scratching, which indicated that **3** and **4** were mainly recovered (Figure S13, Supporting Information).

(B). C-to-C. PXRD patterns for **1γ** and **2β** before and after heating and grinding, respectively, were investigated.

When crystal **1γ** was heated at 80 °C, the PXRD pattern for **1γ** changed to a new one consistent with that for crystal **1β**. This result indicated that a thermal transformation from **1γ** to **1β** took place. By grinding, the PXRD pattern for **2β** altered to

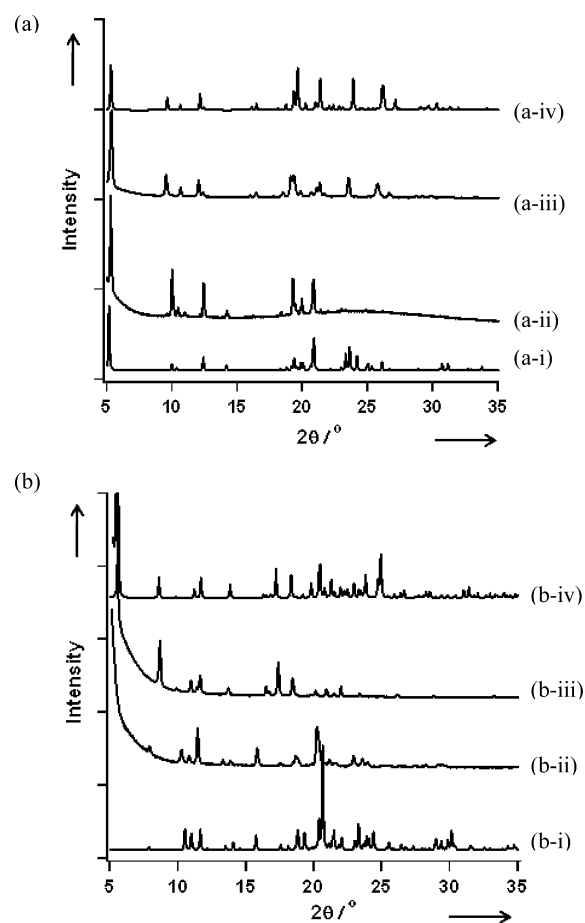


Figure 8. PXRD patterns of **1γ** (a) and **2β** (b). For (a), the simulation patterns for **1γ** (a-i) and **1β** (a-iv), and PXRD patterns before (a-ii) and after (a-iii) heating crystal at 80 °C, and for (b), simulation patterns for **2β**(b-i), **2α** (b-iv), and PXRD patterns before (b-ii) and after (b-iii) grinding of **2β**.

a new one, which was consistent with that for **2α**. This result indicated that the phenyl moiety of **2** rotated from anti to syn position by a mechanical stimulus, grinding. The alterations of PXRD patterns for the samples for both of **1γ** and **2β** induced by thermal and mechanical stimuli, respectively, are shown in Figure 8. IR spectra measurements of **2β** under various conditions also supported the C-to-C transformation from **2β** to **2α** (Figure S14, Supporting Information).

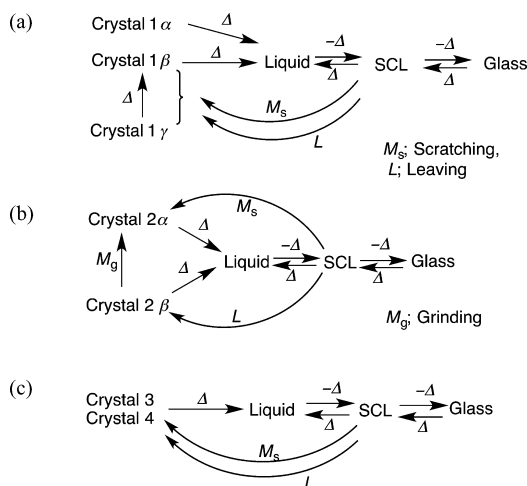
Thermal and Mechanical Phase Transitions. As observed in DSC and PXRD experiments, crystals **1**, **2**, **3**, and **4** showed various thermal phase transitions including transitions in response to the mechanical stimuli, which are summarized in Scheme 1.

It was worth noting that the samples in the SCL state rapidly crystallized by a mechanical stimulus, scratching, and the produced crystals in **1** and **2** were mixture of polymorphs, **1β** and **1γ**, and **2α** having HB structure, which might be kinetically stable.

CONCLUSION

TFMAQ-Ph derivatives having methyl (**1**), ethyl (**2**), isopropyl (**3**), and phenyl (**4**) substituents were prepared as a new type of external stimuli responsive fluorophore. The TFMAQ-Ph derivatives were obtained as single crystals, in which **1** and **2** provided three (**1α**, **1β**, and **1γ**) and two (**2α** and **2β**)

Scheme 1. Phase Transitions of 1 (a), 2 (b), and 3 and 4 (c) by Heating (Δ) and Cooling ($-\Delta$) Processes^a



^a M_s , M_g , and L indicate giving mechanical stimuli, scratching and grinding, and leaving for a long time, respectively.

polymorphs, respectively, having different molecular arrangements. The obtained polymorphs showed C-to-C transformation from **1 γ** to **1 β** and from **2 β** to **2 α** induced by heat and grinding, respectively, with an alteration of emission color. In addition, **4** showed a crystal phase transition between 173 and 90 K. These four fluorophores, **1**, **2**, **3**, and **4**, exhibited characteristic alterations of emission intensity through SCL-to-C transformation induced by mechanical stimuli. After melting, the molecules formed the SCL and G states at room temperature, and those in the SCL state rapidly crystallized by scratching. **1**, **2**, **3**, and **4** in the SCL state were confirmed to mechanically provide a mixture of crystals, **1 β** and **1 γ** , only **2 α** , **3**, and **4**, respectively, by PXRD patterns. The emissions in the SCL state were weak, while those in the solid state were intense. By taking advantage of the alteration of emission intensity caused by SCL-to-C transformation, we could “write” and “erase” letters with the cycle of scratching and heating. Use of the SCL-to-C transformation with a tuned emitting intensity (write and erase) might be a useful approach for switchable emitting materials.

EXPERIMENTAL SECTION

General Methods. Infrared spectra were recorded on a JASCO 420 FT-IR spectrometer. ¹H and ¹³C NMR spectra were measured on a Bruker Biospin AVANCE III 500 and Varian 500 Fourier transform spectrometer using CDCl₃ and CD₂Cl₂ as solvent and referenced to TMS (Figure S15, Supporting Information). Differential scanning calorimetry (DSC) curves were recorded by a SII SSC 5200 and 7000, and NETZSCH DSC200 F3. Fast atom bombardment mass spectra (FAB MS) were recorded on a JEOL JMS-SX102 spectrometer. Electron spray mass spectra (ESI MS) were recorded on a Bruker Daltonics microTOF spectrometer. Melting points were obtained with a MEL-TEMP heating block and are uncorrected. Elemental analyses were performed at the Analytical Center of the Faculty of Science in Kyushu University.

X-ray Crystallography. Single-crystal X-ray diffraction (SXRD) data and experimental details are summarized in Table S1, Supporting Information for crystal **1 α** , **1 β** , and **1 γ** , Table S2 for **2 α** , **2 β** , and **3**, and Table S3 for **4** at various temperatures. Suitable single crystals were glued onto a glass fiber using epoxy resin. All SXRD data were collected on a Bruker AXS APEX-II diffractometer with graphite monochromated MoK α radiation ($\lambda = 0.71069$ Å). The molecular

structures were solved by direct methods (SIR 92²³ or SHELXL 97²⁴ or SIR 2004²⁵). The refinements were converged using the full-matrix least-squares method from the Crystal Structure software package²⁶ to give P $\bar{1}$ (No. 2), C2/c (No. 15), Cc (No. 9), Pna2₁ (No. 33), P $\bar{1}$ (No. 2), P2₁/c (No. 14), P $\bar{1}$ (No. 2), and C2/c (No. 15) for crystals, **1 α** , **1 β** , **1 γ** , **2 α** , **2 β** , **3**, **4**,₁₇₃, and **4**,₉₀, respectively. All non-hydrogen atoms were refined anisotropically and hydrogen atoms were refined isotropically. Crystallographic data for the structure reported in this paper have been deposited with the Cambridge Crystallographic Data Center as supplementary publications nos. CCDC 917133, 917134, 917135, 980547, 980548, 980549, 980550, and 980551 for crystals, **1 α** , **1 β** , **1 γ** , **2 α** , **2 β** , **3**, **4**,₉₀, and **4**,₁₇₃, respectively. Powder X-ray diffraction (PXRD) spectra were performed with a Bruker AXS D2PHASER. PXRD measurements for the crystal and powder samples were carried out at a 2θ angle of 5–50° at 25 °C.

Absorption and Emission Spectra and Fluorescence Quantum Yield Measurements. In the measurement of the solution sample, the compounds were dissolved in the solvents and nitrogen gas was bubbled through the needle. Roughly crushed crystals and ground crystals were used as crystal and powdered samples, respectively. UV–vis spectra were recorded on a JASCO V570 spectrometer. The absorption spectra of the powder samples diluted by KBr were obtained by the measurements of the diffractive reflection spectra followed by Kubelka–Munk conversion using a JASCO ISN-470 integrating sphere assembly. The fluorescence spectra were recorded on a PerkinElmer LS 50B spectrometer. The fluorescence quantum yield was determined with Hamamatsu C9920-01 instruments equipped with a CCD by using a calibrated integrating sphere system.

Materials. 2,4-Di(trifluoromethyl)-7-phenylaminoquinoline (TFMAQ-Ph) was prepared by the procedure reported previously.⁷

2,4-Di(trifluoromethyl)-7-methylphenylaminoquinoline, 1. Sodium hydride (27 mg, 1.1 mmol) was added to a solution of TFMAQ-Ph (0.20 g, 0.56 mmol) in THF (4 mL) with stirring. The suspension was stirred for 20 min, and then methyl iodide (0.32 g, 2.25 mmol) was added. The solution was stirred at room temperature for 6 h. The reaction mixture was poured into water and extracted three times with ether (60 mL). Organic layers were combined, dried over MgSO₄, and evaporated under reduced pressure. Crude residue was chromatographed on a silica gel using *n*-hexane/ether = 50:1 as eluents to separately afford a pale yellow solid (0.18 g, 0.49 mmol) in 87% yield. Mp 93 °C, ¹H NMR (500 MHz, CD₂Cl₂) δ 7.89 (*dd*, $J = 9.4$ and 2.1 Hz, 1H), 7.70 (*s*, 1H), 7.48 (*d*, $J = 2.1$ Hz, 1H), 7.45 (*d*, $J = 8.6$ Hz, 2H), 7.32 (*dd*, $J = 9.4$ and 2.6 Hz, 1H), 7.30 (*m*, 3H), and 3.49 (*s*, 3H) ppm. ¹³C NMR (127 Hz, CD₂Cl₂) δ 151.56, 151.00, 147.73, 147.11, 136.00, 130.47, 126.92, 126.69, 126.59, 124.46, 122.71, 120.68, 117.67, 110.32, 109.61, and 40.93 ppm. FAB MS (in *m*-NBA matrix), 370 [1]⁺. Anal. Calcd for C₁₈H₁₂N₂F₆: C 58.38, H 3.27, N 7.57%; Found: C 58.20, H 3.32, N 7.59%.

2,4-Di(trifluoromethyl)-7-ethylphenylaminoquinoline, 2. Fluorophore **2** was prepared in a manner similar to the procedure for **1** by using ethyl iodide in place of methyl iodide. Crude residue was chromatographed on a silica gel using *n*-hexane/EtOAc = 100:1 as eluents to separately afford a pale yellow solid in a quantitative yield. Mp 69 °C (from DSC), ¹H NMR (500 MHz, CD₂Cl₂) δ 7.87 (*dd*, $J = 9.5$, 1.9 Hz, 1H), 7.67 (*s*, 1H), 7.47 (*t*, $J = 7.8$ Hz, 1H), 7.41 (*d*, $J = 2.6$ Hz, 1H), 7.32 (*t*, $J = 7.5$ Hz, 1H), 7.27 (*d*, $J = 7.4$ Hz, 2H), 7.24 (*d*, $J = 7.4$ Hz, 2H), 3.95 (*q*, $J = 7.1$ Hz, 2H), and 1.32 (*t*, $J = 7.1$ Hz, 3H) ppm. ¹³C NMR (126 MHz, CD₂Cl₂) δ 151.23, 150.87, 147.80, 145.96, 136.03, 130.73, 127.92, 127.03, 124.91, 124.53, 123.13, 120.86, 117.55, 110.21, 109.29, 47.69, and 12.43 ppm. ESI-MS, 407.1 [2 + Na]⁺. Anal. Calcd for C₁₉H₁₄N₂F₆: C 59.38, H 3.67, N 7.29%; Found: C 59.66, H 3.97, N 7.07%.

2,4-Di(trifluoromethyl)-7-isopropylphenylaminoquinoline, 3. Fluorophore **3** was prepared in a manner similar to the procedure for **1** by using 2-iodopropane in place of methyl iodide. Crude residue was chromatographed on a silica gel using *n*-hexane/EtOAc = 100:1 as eluents to separately afford a pale yellow solid in a quantitative yield. Mp 94 °C (from DSC), ¹H NMR (500 MHz, CDCl₃) δ 7.82 (*dd*, $J = 9.6$ and 2.0 Hz, 1H), 7.64 (*s*, 1H), 7.49 (*m*, 2H), 7.42 (*m*, 2H), 7.17 (*d*,

$J = 8.5$ Hz, 2H), 4.52 (*quin*, $J = 6.6$ Hz, 1H), and 1.24 (*d*, $J = 6.5$ Hz, 3H) ppm. ^{13}C NMR (126 MHz, CDCl_3) δ 151.59, 151.11, 148.15, 141.37, 136.24, 135.99, 131.80, 128.35, 124.71, 124.51, 122.79, 120.66, 117.11, 109.89, 108.14, 49.28, and 21.31 ppm. ESI-MS, 421.3 [3 + Na] $^+$. Anal. Calcd for $\text{C}_{20}\text{H}_{16}\text{N}_2\text{F}_6$: C 60.30, H 4.05, N 7.03%; Found: C 60.37, H 4.07, N 7.00%.

2,4-Di(trifluoromethyl)-7-diphenylaminoquinoline, 4. TFMAQ-Ph (200 mg, 0.56 mmol), tri-*tert*-butylphosphine (11 mg, 10 mol %), palladium acetate (6.3 mg, 5 mol %), potassium *tert*-butoxide (94 mg, 0.84 mmol) were placed on the Schlenk flask and degassed toluene (2 mL) was added. Bromobenzene (188 mg, 1.2 mmol) was added under nitrogen atmosphere, and the reaction mixture was heated at 110 °C for 6 h. Crude residue was chromatographed on a silica gel using *n*-hexane/EtOAc = 300:1–200:1 as eluents to afford a pale yellow solid (230 mg, 0.53 mmol) in 95% yield. Mp 118 °C (from DSC), ^1H NMR (500 MHz, CDCl_3) δ 7.96 (*d*, $J = 9.3$ Hz, 1H), 7.74 (*s*, 1H), 7.64 (*d*, $J = 1.8$ Hz, 1H), 7.55 (*dd*, $J = 9.4$ and 1.9 Hz, 1H), 7.36 (*d*, $J = 7.6$ Hz, 2H), 7.35 (*d*, $J = 7.6$ Hz, 2H), 7.21 (*d*, $J = 8.2$ Hz, 4H), and 7.18 (*m*, 1H). ^{13}C NMR (126 MHz, CDCl_3) δ 151.26, 150.59, 148.35, 146.53, 136.40, 130.44, 126.69, 126.31, 125.87, 124.79, 122.38, 120.47, 119.40, 117.22, and 111.55 ppm. ESI-MS, 455.1 [4 + Na] $^+$. Anal. Calcd for $\text{C}_{23}\text{H}_{14}\text{N}_2\text{F}_6$: C 63.89, H 3.26, N 6.48%; Found: C 64.07, H 3.25, N 6.54%.

■ ASSOCIATED CONTENT

Supporting Information

Photographs of crystals for 1–4, crystallographic data for 1–4 including ORTEP drawings, molecular arrangements, selected bond lengths and angles, Harshfeld fingerprint plots, photophysical data in solution and solid state for 1–4, DSC curves for 1 β , 1 γ , and 2 β , alteration of fluorescence spectra and photographs (irradiating at 365 nm) in the SCL state after scratching for 2–4, PXRD patterns for 3 and 4, IR spectra before and after grinding for 2 β , and ^1H and ^{13}C NMR spectra for 1–4. These materials are available free of charge via the Internet at <http://pubs.acs.org>. Full crystallographic data (CCDC-917133, 917134, 917135, 980547, 980548, 980549, 980550, and 980551 for crystals, 1 α , 1 β , 1 γ , 2 α , 2 β , 3, 4 $_{90}$, and 4 $_{173}$, respectively) have been deposited at the Cambridge Crystallographic Database Center and are available on request from the Director, CCDC, 12 Union Road, Cambridge, CB2 1EZ, UK (Fax: +44-1223-336-033; E-mail: deposit@ccdc.cam.ac.uk or <http://www.ccdc.cam.ac.uk>).

■ AUTHOR INFORMATION

Corresponding Author

*Tel: 81-92-642-6590. Fax: 81-92-642-6590. E-mail: koga@fc.phar.kyushu-u.ac.jp.

Notes

The authors declare no competing financial interest.

■ ACKNOWLEDGMENTS

This work was supported by a Grant-in-Aid for Scientific Research (B)(2)(No. 25288038) from the Ministry of Education, Science, Sports and Culture, Japan, and partially supported by Platform for Drug Discovery, Informatics, and Structural Life Science from the Ministry of Education, Culture, Sports, Science and Technology, Japan.

■ REFERENCES

(1) Goushi, K.; Yoshida, K.; Sato, K.; Adachi, C. *Nat. Photonics* **2012**, *6*, 253–258.
 (2) (a) Zhao, D.; Li, J.; Yang, T.; He, Z. *Biosens. Bioelectron.* **2014**, *52*, 29–35. (b) Perea-López, N.; Elías, A. L.; Berkdemir, A.; Castro-Beltrán, A.; Gutiérrez, H. R.; Feng, S.; Lv, R.; Hayashi, T.; López-Urías,

F.; Ghosh, S.; Muchharla, B.; Talapatra, S.; Terrones, H.; Terrones, M. *Adv. Funct. Mater.* **2013**, *23*, 5511–5517.

(3) O'Carroll, D.; Lieberwirth, I.; Redmond, G. *Nat. Nanotechnol.* **2007**, *2*, 180–184.

(4) (a) Seki, T.; Kurenuma, S.; Ito, H. *Chem.—Eur. J.* **2013**, *19*, 16214–16220. (b) Sagara, Y.; Mutai, T.; Yoshikawa, I.; Araki, K. *J. Am. Chem. Soc.* **2007**, *129*, 1520–1521.

(5) (a) Gu, X.; Yao, J.; Zhang, G.; Yan, Y.; Zhang, C.; Peng, Q.; Liao, Q.; Wu, Y.; Xu, Z.; Zhao, Y.; Fu, H.; Zhang, D. *Adv. Funct. Mater.* **2012**, *22*, 4862–4872. (b) Luo, X.; Li, J.; Li, C.; Heng, L.; Dong, Y.-Q.; Liu, Z.; Bo, Z.; Tang, B. *Z. Adv. Mater.* **2011**, *23*, 3261–3265. (c) Mutai, T.; Satou, H.; Araki, K. *Nat. Mater.* **2005**, *4*, 658–687.

(6) (a) Seki, T.; Sakurada, K.; Ito, H. *Angew. Chem., Int. Ed.* **2013**, *52*, 12828–12832. (b) Kwon, M. S.; Gierschner, J.; Yoon, S.-J.; Park, S. Y. *Adv. Mater.* **2012**, *24*, 5487–5492. (c) Zhang, G.; Lu, J.; Sabat, M.; Fraser, C. L. *J. Am. Chem. Soc.* **2010**, *132*, 2160–2162. (d) Sagara, Y.; Kato, T. *Angew. Chem., Int. Ed.* **2008**, *47*, 5175–5178.

(7) Abe, Y.; Karasawa, S.; Koga, N. *Chem.—Eur. J.* **2012**, *18*, 15038–15048.

(8) (a) Harada, N.; Karasawa, S.; Matsumoto, T.; Koga, N. *Cryst. Growth Des.* **2013**, *13*, 4705–4713. (b) Harada, N.; Abe, Y.; Karasawa, S.; Koga, N. *Org. Lett.* **2012**, *14*, 6282–6285.

(9) (a) Zeidan, T. A.; Trotta, J. T.; Chiarella, R. A.; Oliveira, M. A.; Hickey, M. B.; Almarsson, Ö.; Remenar, J. F. *Cryst. Growth Des.* **2013**, *13*, 2036–2046. (b) López-Mejías, V.; Kampf, J. W.; Matzger, A. J. *J. Am. Chem. Soc.* **2012**, *134*, 9872–9875. (c) Reany, O.; Kapon, M.; Botoshansky, M.; Keinan, E. *Cryst. Growth Des.* **2009**, *9*, 3661–3670. (d) Braum, D. E.; Gelbrich, T.; Kahlenberg, V.; Tessadri, R.; Wieser, J.; Griesser, U. J. *J. Pharm. Sci.* **2009**, *98*, 2010–2026.

(10) (a) Debenedetti, P. G.; Stillinger, F. H. *Nature* **2001**, *410*, 259–267. (b) Noda, T.; Shirota, Y. *J. Am. Chem. Soc.* **1998**, *120*, 9714–9715.

(11) Imanari, M.; Tsuchiya, H.; Seki, H.; Nishikawa, K.; Tashiro, M. *Magn. Reson. Chem.* **2009**, *47*, 67–70.

(12) Yasuda, T.; Shimizu, T.; Liu, F.; Ungar, G.; Kato, T. *J. Am. Chem. Soc.* **2011**, *133*, 13437–13444.

(13) (a) Hunter, C. A.; Lawson, K. R.; Perkins, J.; Urch, C. J. *J. Chem. Soc., Perkin Trans. 2* **2001**, 651–669. (b) Gavezzotti, A.; Desiraju, G. R. *Acta Crystallogr., Sect. B* **1989**, *45*, 473–482.

(14) (a) Nishio, M. *Phys. Chem. Chem. Phys.* **2011**, *13*, 13873–13900. (b) Tárkányi, G.; Király, P.; Varga, S.; Vakulya, B.; Soós, T. *Chem.—Eur. J.* **2008**, *14*, 6078–6086.

(15) Macrae, C. F.; Bruno, I. J.; Chisholm, J. A.; Edgington, P. R.; McCabe, P.; Pidcock, E.; Rodriguez-Monge, L.; Taylor, R.; Streek, J.; van de Wood, P. A. *Appl. Crystallogr.* **2008**, *41*, 466–470.

(16) (a) Bakavoli, M.; Rahimizadeh, M.; Feizyadeh, B.; Kaju, A. A.; Takjoo, R. *J. Chem. Crystallogr.* **2010**, *40*, 746–752. (b) Spackman, M. A.; Jayatilaka, D. *CrystEngComm* **2009**, *11*, 19–32. (c) McKinnon, J. J.; Spackman, M. A.; Mitchell, A. S. *Acta Crystallogr.* **2004**, *B60*, 627–668. (d) Wolff, S. K.; Grimwood, D. J.; McKinnon, J. J.; Javatilaka, D.; Spackman, M. *Crystal Explorer 2.0*; University of Western Australia: Perth, Australia, 2007.

(17) (a) Wu, Y.-Y.; Chen, Y.; Gou, G. Z.; Mu, W. H.; Lv, X. J.; Du, M. L.; Fu, W. F. *Org. Lett.* **2012**, *14*, 5226–5229. (b) Grabowski, Z. R.; Rotkiewicz, K.; Rettig, W. *Chem. Rev.* **2003**, *103*, 3899–4032. (c) Soujanya, T.; Fessenden, R. W.; Samanta, A. J. *Phys. Chem.* **1996**, *100*, 3507–3512. (d) Sato, Y.; Morimoto, M.; Segawa, H.; Shimidzu, T. *J. Phys. Chem.* **1995**, *99*, 35–39.

(18) (a) Lippert, E. Z. *Naturforsch.* **1955**, *10A*, 541–545. (b) Lippert, E.; Moll, F. Z. *Elektrochem.* **1954**, *58*, 718–724. (c) Mataga, N.; Kaifu, Y.; Koizumi, M. *Bull. Chem. Soc. Jpn.* **1956**, *29*, 465–470. (d) Onsager, L. J. *J. Am. Chem. Soc.* **1936**, *58*, 1486–1493.

(19) (a) Cheon, J.-D.; Mutai, T.; Araki, K. *Org. Biomol. Chem.* **2007**, *5*, 2762–2766. (b) Becke, A. D. *J. Chem. Phys.* **1993**, *98*, 5648–5652.

(20) (a) Hisaki, I.; Hiraishi, E.; Sasaki, T.; Orita, H.; Tsuzuki, S.; Tohnai, N.; Miyata, M. *Chem.—Asian J.* **2012**, *7*, 2607–2614. (b) Hinoue, T.; Shigenoi, Y.; Sugino, M.; Mizobe, Y.; Hisaki, I.; Miyata, M.; Tohnai, N. *Chem.—Eur. J.* **2012**, *18*, 4634–4643.

- (21) (a) Rice, A. P.; Tham, F. S.; Chronister, E. L. *J. Chem. Crystallogr.* **2013**, *43*, 14–15. (b) Mehta, G.; Sen, S. *Chem. Commun.* **2009**, 5981–5983.
- (22) Ito, H.; Saito, T.; Oshima, N.; Kitamura, N.; Ishizuka, S.; Hinatsu, Y.; Wakeshima, M.; Kato, M.; Tsuge, K.; Sawamura, M. *J. Am. Chem. Soc.* **2008**, *130*, 10044–10045.
- (23) SIR 92: Altomare, A.; Cascarano, G.; Giacovazzo, C.; Guagliardi, A. *J. Appl. Crystallogr.* **1993**, *26*, 343–350.
- (24) SHELX97: Scheldrick, G. M.; Schneider, T. R. *Methods Enzymol.* **1997**, *276*, 319–343.
- (25) SIR 2004: Burla, M. C.; Caliendo, R.; Camalli, M.; Carrozzini, B.; Cascarano, G. L.; De Caro, L.; Giacovazzo, C.; Polidori, G.; Spagna, R. *J. Appl. Crystallogr.* **2005**, *38*, 381–388.
- (26) *Crystal Structure 3.5.2: Crystal Structure Analysis Package*; Rigaku: The Woodlands, TX, 2000-2003; integrating sphere system.